[redacted] Copy 593

NASA TM X-515

NASA TM X-515

[redacted]

UNCLASSIFIED

TO [redacted]

By Authority of [redacted] Date [redacted]

TECHNICAL MEMORANDUM

Declassified by authority of NASA X-515
Classification Change Notices No. 210
Dated **12-15-70

ANALYTICAL INVESTIGATION OF AN ACCELERATION AUTOPILOT FOR CONTROL OF THE IMPACT POINT OF A BALLISTIC MISSILE DURING REENTRY

By Jacob H. Lichtenstein and Terrance M. Carney

Langley Research Center
Langley Field, Va.

[redacted]

NATIONAL AERONAUTICS AND SPACE ADMINISTRATION
WASHINGTON
April 1961

[redacted] CONFIDENTIAL

N

NATIONAL AERONAUTICS AND SPACE ADMINISTRATION

TECHNICAL MEMORANDUM X-515

ANALYTICAL INVESTIGATION OF AN ACCELERATION AUTOPILOT FOR CONTROL OF THE IMPACT POINT OF A BALLISTIC MISSILE DURING REENTRY*

By Jacob H. Lichtenstein and Terrance M. Carney

SUMMARY

An analytical investigation was made of the feasibility of changing the impact point of a ballistic missile by use of aerodynamic controls coupled with a simple acceleration-command system during the terminal phase of the reentry.

The results show that the impact point of the missile system considered in this investigation can be altered by about 10 miles in any direction from the nominal location and that the displacement of the impact point is highly nonlinear with control command; thus, a detailed calibration would be required. The results also show that an integrating servosystem using acceleration feedback for damping would operate satisfactorily throughout the reentry and that there was considerable latitude in the choice of sensitivity and gain constants.

INTRODUCTION

The problem of assuring that the warhead of a ballistic missile will impact at its selected target with a very small error is still a pressing one. Considerable effort is being expended in improving the methods and accuracy of control during the launch phase of the flight in order to make the flight characteristics at injection into the ballistic path as close to the desired values as possible. However, no matter how closely the flight and desired characteristics are made to match, this method cannot compensate for the miss distance that develops due to factors at the terminal phase of the flight. These miss distances result mainly from the lack of precise knowledge of the location of the

target with respect to the launch point, and they are an appreciable part of the total circle of probable error. If, on the other hand, the terminal phase of the missile flight path could be controlled to substantially alter the impact point and compensate for errors, the probability of striking the target would be greatly increased. In addition, such control may make it possible to relax to some extent the stringent steering requirements necessary during the launch phase. For such a system to accomplish its purpose, it must be able to determine the miss distance between its estimated impact point and the target and convert this information to a suitable command. This command is then fed to the control system in such a manner that proper correction can be achieved in the final stage of the reentry.

The investigation presented in this paper is an analytical study of the latter part of the problem, namely, control of a supersonic impact ballistic missile in order to achieve a deviation of its impact point. The error between the target point and the point of impact of the missile in unaltered flight was assumed to have been obtained by some means, such as a map-matching technique. This error was converted to constant-normal-acceleration commands in range and azimuth. These commands were fed to the autopilot which in turn operated aerodynamic controls to achieve the desired normal acceleration. The trajectories of the missile, as it decended through the atmosphere with various amounts of command acceleration in the range or azimuth direction or both, were computed on an IBM type 704 electronic data processing machine. The trajectories were computed for the no-wind condition and for the conditions in which the geostrophic wind was either a head, tail, or side wind.

SYMBOLS

The axis system used in this analysis is shown in figure 1, and the symbols used are defined as follows:

A	cross-sectional area based on maximum body diameter, sq ft
a	acceleration, g units
B_1 to B_5	coefficients of denominator of transfer function, a/a_i
C_m	pitching-moment coefficient, $\frac{\text{Pitching moment}}{QAd}$

C_{m_q}	damping-in-pitch coefficient, $\frac{\partial C_m}{\partial\left(\frac{qd}{2V}\right)}$
C_{m_α}	variation in pitching-moment coefficient with angle of attack, per radian
C_{m_δ}	variation in pitching-moment coefficient with control deflection, per radian
C_X	axial-force coefficient, $\frac{\text{Axial force}}{QA}$
C_{Z_α}	rate of change of side-force coefficient with angle of attack, per radian
C_{Z_δ}	rate of change of side-force coefficient with control deflection, per radian
D	differential operator, $\frac{\partial}{\partial t}$
d	maximum body diameter, ft
E_1 to E_5	coefficients of numerator of transfer equation for integrating servosystem
F_1 to F_5	transfer functions of components of system
F_g	force due to gravity, lb
$\overline{F}$	closed-loop transfer function of inner loop
g	acceleration due to gravity at surface of earth, 32.17 ft/sec^2
h	altitude above surface of earth, ft
I_X	moment of inertia about X-axis, slug-ft^2
I_Y	moment of inertia about Y- or Z-axes, slug-ft^2
K_1	forward loop sensitivity

K_2	damping feedback gain constant
K_3	acceleration feedback gain constant
$K_1' = 57.3K_1$	
$K_2' = 32.17K_2$	
$K_3' = 32.17K_3$	
k	radius of gyration, ft
M	Mach number
m	mass, slugs
p,q,r	angular velocities about X-, Y-, and Z-axes, respectively, radians/sec
Q	dynamic pressure, $\frac{1}{2}\rho V^2$, lb/sq ft
rd/2V	nondimensional pitching-velocity parameter referred to diameter
t	time, sec
u,v,w	components of velocity along X-, Y-, and Z-axes, respectively, ft/sec
V	resultant velocity with respect to air, ft/sec
V_X, V_Y, V_Z	components of geostrophic wind along X-, Y-, and Z-axes, respectively, ft/sec
W	magnitude of the geostrophic wind, ft/sec
X,Y,Z	reference axes with orgin at center of mass of body with X-axis alined along line of symmetry
X_i, Y_i, Z_i	reference axes with origin on earth surface directly under point where trajectory altitude is 200,000 feet

x,y,z	distance from the origin along X_i-, Y_i-, and Z_i-axes, respectively, to center of gravity of vehicle, ft or nautical miles
α	angle of attack, radians
δ	control deflection, radians
ζ	damping ratio of instrument (ratio of actual damping to critical damping)
θ,ψ	Euler angles defined in figure 1, radians or deg
ρ	density of air, slugs/cu ft
ϕ	angular displacement about X-axis, radians
$\bar{\psi}$	direction of geostrophic wind relative to X_i-axis
ω_n	natural frequency of instrument, radians/sec

Subscripts:

a	in azimuth direction
cg	center-of-gravity location
e	error signal
i	input
n	at nose location
r	in range direction

A dot over a symbol indicates differentiation with respect to time.

DESCRIPTION OF THE METHOD

As mentioned in the introduction, it is assumed that some method, such as a map-matching technique, is available to establish the error between the target point and the projected impact point of the missile on its unaltered flight path. These error signals are converted to constant-acceleration commands to the control system. These command signals can be in either the range or azimuth direction or a combination

of both. This portion of the operation is assumed to have taken place at an altitude above 200,000 feet. At 200,000 feet the control system is activated and the previously determined command signal generally is maintained down to impact.

The vehicle considered in this investigation was a truncated-cone, flared-cylinder body (fig. 2) which is representative of a missile which normally impacts at a Mach number of about 2. For the purpose of this report, any aerodynamic control capable of developing the required trim moments would be suitable. A representative control configuration, which was based upon altering the flare angle of segments of the skirt flare, was chosen. The movable segments on the top and bottom of the missile were coupled and the segments on the two sides were coupled so that when one increased its flare angle the opposite segment decreased its flare angle. (See fig. 2.) These control surfaces moved in response to the error signal between the input command acceleration and the actual acceleration achieved by the missile. The aerodynamic derivatives used for the missile were the best estimates from data available at the start of the program. The control derivatives C_{Z_δ} and C_{m_δ}, for which there were no test data, were computed by Newtonian impact theory by the method described in reference 1. (However, since no effect of shielding of the control on the lee side of the body at high angles of attack was included, these derivatives are only approximate values.) The mass data, aerodynamic derivatives, and initial conditions are presented in table I. The equations of motion of the missile are presented in appendix A along with the conditions for the computations.

For the present investigation, a flat earth was assumed. It is believed that for the relatively steep reentry of an intercontinental ballistic missile no serious loss in generality would result because the total travel during the controlled flight would be less than 200 miles.

CONTROL SYSTEMS

In this investigation only yaw- and pitch-control systems are considered. Two identical systems control the missile in pitch and yaw and are termed, respectively, the range and azimuth controls. In practice a third control system would be required; this would be a roll-control system whose sole function is to prevent the missile from acquiring any displacement in the angle of roll and from developing any rate of roll and thus insure that the range controls are always in the vertical plane. For the purposes of the investigation it was assumed that the response of the roll-control system was very rapid so that essentially the rate of roll as well as the angle of roll is kept to zero at all times. Therefore, dynamic coupling of this system with the range and azimuth systems was not considered.

As an example of the main control systems a block diagram of the pitch-control system as used in this investigation is shown in figure 3. The control servomechanism is an integrating hydraulic servo which will give a control deflection proportional to the integral of the error signal and, therefore, will hold a trim deflection when the error signal is zero. The natural frequency of this servo is so high that its dynamics could safely be neglected. Two accelerometers in each plane, one located in the nose and one at the center of gravity, are used as sensors. The accelerometer signals were differenced to determine angular acceleration which when fed to the integrating servo provided the damping. This control system is similar to the one described in reference 2. The location of the control-system components within the missile is shown in figure 2. Reasonable assumptions were made for the components of this system. The servo has a piston with an area of 2.5 square inches operating under a pressure of 2,000 pounds per square inch. The hydraulic fluid is obtained from a high-pressure reservoir having a capacity of 2.11 cu ft. The rate of control deflection was limited to 0.4 radian per second by the assumed maximum rate of flow of hydraulic fluid through the servo-control valve of 8 gallons per minute. The used fluid was ejected rather than recycled because the additional complication of the mechanization did not seem warranted. The accelerometers were considered to be identical to each other. The mathematical expressions for the servo and accelerometer models are given in appendix A.

COMPUTATIONS

The motion of the missile as it descended through the atmosphere acting under the variously imposed control commands was computed. The computations were initiated at 200,000 feet and continued to the ground, and the initial conditions were those that a representative intercontinental ballistic missile would have at that altitude. The geostrophic wind conditions were actually imposed at an altitude of 400,000 feet where they were first considered to be significant, and the missile was considered to be a passive body down to 200,000 feet. The range and azimuth input commands varied from -10g to 10g individually and in combination. A list of the various runs and their conditions is given in table II. It was found early in the program that for large positive commands in range (tending to increase the range) the missile lost so much velocity that its forward speed became subsonic while it was still more than 2 minutes and 10 miles away from the target; thus, its vulnerability to countermeasures was increased. Therefore, for those runs with a positive range command of 5g or 10g, this command was reduced to 0g when the missile had pitched up from its initial reentry angle of $-22\frac{1}{2}^{\circ}$ to about 0°.

In order to insure that suitable gain constants were used for the servo sensitivity and damping feedback loop, the dynamic response of the system was studied on both digital and analog computers for various gain constants and for conditions at various altitudes along a representative trajectory. (See table III.) A quasi-static analysis technique was used, in which it was assumed that if good stability could be assured statically for any dynamic pressure and altitude to be encountered on a typical trajectory, the rate of change of these conditions in the real case would not cause instability. For the digital computations the nonlinear equations of motion in appendix A were linearized in the manner discussed in appendix B, and the loci of the roots of the system were computed. The stability results obtained by the root-locus analysis were checked by analog computations by use of the nonlinear equations of motion presented in appendix A. A maximum normal acceleration of 10g was selected because it was believed that this would be a reasonable value that the missile could manage without risking damage to the structure from the concentrated mass of the heavy bomb. The maximum control deflection of 10° was selected because at this deflection one or the other of the control segments would have retracted to a flare angle of 0°. This maximum control deflection permits a maximum trim angle of attack of 9.6°. Both the trajectories and roots of the stability equations were computed on an IBM type 704 electronic data processing machine.

The aerodynamic derivatives used for this model were obtained from wind-tunnel tests on models of similar shape or computed by use of the Newtonian impact theory. The value for the damping derivative C_{m_q} was obtained from the results of some preliminary oscillation tests on a similar model which were available at the time. The values of C_{m_α}, C_{Z_α}, C_{m_δ}, and C_{Z_δ} were computed by use of the impact theory for the basic missile with the controls undeflected. The effect of shielding of the leeward surfaces at angles of attack was not considered. The value of C_{m_δ} was reduced by 1/2 because it had been found in reference 3 that Newtonian impact theory overestimated the value by a factor of about 2 over the angle-of-attack range of interest.

RESULTS AND DISCUSSION

Presentation of Results

The results of this investigation are presented in figures 4 to 12. Figure 4 presents plots of the loci of the roots of the stability equation for various gain factors for the integrating servosystem used in this investigation for the condition of highest dynamic pressure.

Figure 5 presents a map of the roots of the characteristic equation for the gains used in the trajectory studies $\left(K_1' = 6;\ K_2' = 6\right)$ for all six of the representative flight conditions selected for the quasi-static investigation. Figure 6 presents the stability boundaries determined from the analog study for the same flight conditions. Figures 7, 8, and 9 present some typical trajectories for various amounts of range control for an earth-fixed-axis system. Figure 10 shows the drift due to geostrophic wind for the case for no control in both range and azimuth. Figure 11 shows a similar displacement of impact point due to earth-rotation effects including geostrophic wind. Figure 12 presents maps of the impact points for various amounts of control for conditions of no earth-rotation effects, and for reentry against, with, and normal to the direction of earth rotation.

Discussion

Control system - missile stability.- The stability of the control-system, missile combination was initially investigated by the root-locus technique. A closed-loop transfer function for the acceleration response to a command acceleration was written for the linearized system. The associated characteristic equation was factored for six flight conditions and a range of gain constants, and the resulting roots were plotted. This investigation was checked and extended by programming the nonlinear equations on the analog computer for the various static flight conditions. The transient response for a step command in acceleration was evaluated qualitatively and correlated with the root-locus results.

For the root-locus analysis, where linearized equations of motion are used and the velocity and altitude are considered constant, the transfer function for the overall system is of the following form:

$$\frac{a}{a_i} = \frac{K_1\left(E_1D^4 + E_2D^3 + E_3D^2 + E_4D + E_5\right)}{D^5 + B_1D^4 + B_2D^3 + B_3D^2 + B_4D + B_5}$$

The terms E_1 to E_5 and B_1 to B_5 are constants whose values depend upon aerodynamic terms of the missile, coefficients of the instruments (such as accelerometers), and the gain and sensitivity constants used in the system. The equations and terms are described in appendix B.

The data presented in figure 4 are the loci of the roots of the characteristic equation of the integrating servosystem for a variation

of the damping gain factor K_2' for several values of the forward sensitivity of the system K_1' for the flight condition 1 listed in table III. For low values of the sensitivity K_1 the response is slow, as indicated by a small value of the root located on the negative real axis, and for low values of the damping gain K_2 the low-frequency oscillation is undamped (the complex roots closest to the origin). When both the sensitivity and damping gain are high, the high-frequency oscillation becomes unstable. There is considerable latitude in the choice of sensitivity and damping gain that would result in a stable system with reasonable response time. Similar results were obtained for the other flight conditions, and on the basis of this digital study the constants $K_1' = 6$ for the servo sensitivity and $K_2' = 6$ for the feedback gain were picked for all the trajectory computations.

Figure 5 presents a map of the roots of the system for $K_1' = 6$ and $K_2' = 6$ for all the flight conditions studied. As might be expected, the response becomes slow as the dynamic pressure decreases, but the system shows good stability characteristics at all flight conditions.

For the analog study the complete equations of motion given in appendix A were used with the exceptions that the dynamic pressure and velocity were held constant. The two gain constants, servo sensitivity and damping feedback, were varied independently and the qualitative boundaries for satisfactory response to commands in range and azimuth were obtained. (See fig. 6.) These boundaries were virtually unchanged for pitch, yaw, or combined commands; therefore, only the pitch cases are presented. The results presented in figure 6 substantiate the results of the root-locus study. The gain constants $K_1' = 6$ and $K_2' = 6$ result in satisfactory performance for all of the flight conditions investigated.

Trajectory considerations.- In the section describing computations, some difficulties which might be encountered with large positive range commands were mentioned; therefore, reducing this command at some point along the trajectory would be desirable. The trajectory plots presented in figures 7 to 9 show why this was considered necessary. For the case in which the maximum positive command was maintained down to impact, the missile actually reverses its descent and increases its altitude by a considerable amount before its final descent to impact. In the process of going through this maneuver the missile sustains such a large loss in velocity that it becomes subsonic. The points at which the missile velocity first falls below a Mach number of 2 and of 1, and the time

to go to impact from these points are indicated in the figures. For the 10g positive command the missile spends about $2\frac{3}{4}$ minutes below a Mach number of 2 and about 2 minutes below a Mach number of 1. This situation makes the missile very vulnerable to countermeasures and thus would nullify the prime purpose for use of a supersonic-impact missile. Cutting back the range command to 0g when the missile pitches up to a horizontal attitude causes the time the missile spends at these slow speeds to be reduced to the point where it no longer appears to be such a serious objection. In order to achieve this improvement in the time spent at low speeds it was necessary to sacrifice some range capability of the missile. In all of the data presented for the remainder of the paper this modified command system was used.

The effect on the impact point of accounting for the earth rotation and consequent geostrophic wind is shown in figures 10 and 11 for the no-control condition. For the no-rotation, no-wind case both the earth rotation and geostrophic wind were neglected. For the other cases, however, the earth rotation introduces two effects, a movement of the target point in the direction of the rotation and a drift of the missile from its inertial path due to the geostrophic wind. The wind-drift increment alone is shown in figure 10 for reentry with, against, or normal to the earth rotation, and the magnitude of this drift is about 3 miles in the direction of the wind. The data presented in figure 11 include both earth-rotation effects, that is, the movement of the target point and the wind drift. The data show that the impact points are displaced about 5 miles in a direction which is opposite to the direction of earth rotation. This displacement results from the fact that the loss in range measured in an earth-fixed-axis system (moving with the earth) for a reentry in the same direction as the earth rotation is larger than the gain in range due to the geostrophic wind drift. For reentry against the rotation, the gain in range in an earth-fixed-axis system is larger than the loss due to wind drift. Although not presented, the results for the 0g command and the no-control cases are essentially the same. This fact is attributable to the missile aerodynamics. The normal directional stability of the missile will turn it into the relative wind so that there will be no transverse forces. The 0g command has the effect mainly of augmenting the directional stability of the missile to hasten this effect slightly and tends to damp the oscillation in angle of attack about the relative wind. The drift results from the component of the drag in the geostrophic-wind direction.

For the uncontrolled missile these displacements are easily corrected by altering the direction in which the missile is launched to accommodate the displacement. For the controlled missile, however, it is necessary to use the proper set of maps showing deflection plotted against command for the direction and magnitude of the geostrophic wind at the reentry location.

Effect of Control on Impact Point

The data presented in figure 12 are maps of the displacement of the impact point for various command inputs for the four conditions of no-earth rotation, and for reentry against, with, and normal to earth rotation. For the no-wind, head-wind, and tail-wind cases the map would be symmetrical about the Z-axis; therefore, only one side is presented. Two of the most significant facts which are apparent from the data on these figures are the nonlinearity in magnitude of the displacement of the impact point with command from the basic impact point (0g command in range and azimuth), and the sizable loss in range with azimuth command for the same range command. This irregular behavior of the impact-point displacement with command signal indicates that perhaps a second map-matching operation with the existing equipment and a proper displacement-command map of the target area be used to determine the required command signal in order to bring about the desired change in the impact point, rather than the use of a complicated mechanical or computational procedure.

In addition to the basic data a circle of 10-mile radius is shown with the center at 0g azimuth, 2g range command. For all of the wind conditions this circle is almost entirely within the limits of the displacement pattern. Therefore, if the control system were biased so that a command of 0g azimuth, 2g range would be required to hit the nominal target, the system considered herein would have the capability of making a 10-mile correction in almost any direction.

These maps were made for reentry at the equator where the earth-rotation effects are greatest. For any other impact point the geostrophic effects would be smaller. The resulting map, therefore, would show a smaller variation from the no-earth-rotation map. Some error may be introduced by the lack of exact knowledge of the direction and magnitude of the geostrophic wind at the impact point, but this should be small.

CONCLUSIONS

An analytical investigation of control of the impact point of a typical supersonic-impact ballistic missile by use of aerodynamic controls coupled with a simple acceleration-command system during the terminal phase of its flight has indicated the following conclusions:

1. For a maneuver limitation of 10g, the impact point can be altered from the nominal impact point by about 10 nautical miles in range, azimuth, or a combination of both.

2. The variation of impact point with command signal is highly nonlinear; therefore, determination of the proper command for the desired change of the impact point would require detailed calibration relating the predicted error to the desired command.

3. An integrating servo control using acceleration feedback for damping would operate satisfactorily, that is, with good damping and a reasonable response time, with one set of constants for the control sensitivity and damping gain throughout the flight.

L
1
3
3
4

Langley Research Center,
National Aeronautics and Space Administration,
Langley Field, Va., January 19, 1961.

[redacted]

[redacted]

APPENDIX A

EQUATIONS OF MOTION FOR THE MISSILE AND CONTROL-SYSTEM COMPONENTS

The equations used in computing the motions of the missile in response to a command input are given in this appendix. A block diagram of the range- or pitch-control system is shown in figure 3, and the azimuth- or yaw-control system is identical to the pitch system.

Equations of Motion

The equations of motion of the missile are in a body-axis system (fig. 1). The X-axis is always aligned with the axis of symmetry and the Z-axis is constrained to remain in a plane parallel to the $X_i Z_i$ inertial plane. This constraint insures that the range controls always operate in a vertical plane and the azimuth controls operate perpendicular to this plane. The equations used to describe the missile motion are as follows:

For the X-force equation,

$$\dot{u} = \frac{QA}{m} C_X + rv - qw - g \sin \theta$$

where $C_X = C_{X,\alpha=0^\circ} \cos \alpha$, and $C_{X,\alpha=0^\circ}$ is axial-force coefficient at $\alpha = 0^\circ$. $C_{X,\alpha=0^\circ}$ is modified by $\cos \alpha$ to simulate the variation with angle of attack.

For the Y-force equation,

$$\dot{v} = \frac{QA}{m}\left[C_{Z_\alpha}\left(\frac{v - V_Y}{V}\right) + C_{Z_\delta}\delta_r\right] + qw \tan \theta - ru - g \cos \theta$$

For the Z-force equation,

$$\dot{w} = \frac{QA}{m}\left[C_{Z_\alpha}\left(\frac{w - V_Z}{V}\right) + C_{Z_\delta}\delta_a\right] + qu - qv \tan \theta$$

[redacted]

For the Y-moment equation,

$$\dot{q} = \frac{QAd}{I_Y}\left[C_{m_\alpha}\left(\frac{w - V_Z}{V}\right) + C_{m_q}\frac{qd}{2V} + C_{m_\delta}\delta_a\right] + \left(1 - \frac{I_X}{I_Y}\right)rq \tan\theta$$

For the Z-moment equation,

$$\dot{r} = \frac{QAd}{I_Y}\left[-C_{m_\alpha}\left(\frac{v - V_Y}{V}\right) + C_{m_q}\frac{rd}{2V} - C_{m_\delta}\delta_r\right] + \left(\frac{I_X}{I_Y} - 1\right)q^2\tan\theta$$

The missile roll stabilization is simulated by making both ϕ and $\dot{\phi}$ equal zero and the expression $\dot{\phi} = p - q \tan\theta$ becomes $p = q \tan\theta$. In addition to the symbols listed previously the following definitions are necessary:

$$\alpha = \arcsin\frac{\sqrt{(v - V_Y)^2 + (w - V_Z)^2}}{V}$$

$$V = \sqrt{(u - V_X)^2 + (v - V_Y)^2 + (w - V_Z)^2}$$

$$\dot{\theta} = r$$

$$\dot{\psi} = -\frac{q}{\cos\theta}$$

$$\dot{x} = u\cos\theta\cos\psi - v\sin\theta\cos\psi - w\sin\psi$$

$$\dot{y} = u\sin\theta + v\cos\theta$$

$$\dot{z} = u\cos\theta\sin\psi - v\sin\theta\sin\psi + w\cos\psi$$

$$V_X = W_{X_i}\cos\psi\cos\theta + W_{Z_i}\sin\psi\cos\theta$$

$$V_Y = -W_{X_i}\cos\psi\sin\theta - W_{Z_i}\sin\psi\sin\theta$$

$$V_Z = -W_{X_i} \sin \psi + W_{Z_i} \cos \psi$$

where

$$W_{X_i} = W \cos \bar{\psi}$$

$$W_{Z_i} = W \sin \bar{\psi}$$

and

$\bar{\psi}$ = Azimuth angle of geostrophic wind

Control System

The equations which define the control motions for the range and azimuth servos are

$$\frac{\delta_r}{a_{e,r}} = -\frac{K_{1,r}}{D}$$

and

$$\frac{\delta_a}{a_{e,a}} = -\frac{K_{1,a}}{D}$$

An integrating servo control was used in order that the existing control deflection would be held for a zero error signal ($a_e = 0$). The four accelerometers used (2 range and 2 azimuth) were considered identical instruments and the equation defining the output for the range and azimuth accelerometers mounted at the center of gravity is

$$\frac{a_{cg,r}}{a_r} = \frac{a_{cg,a}}{a_a} = \frac{\omega_n^2}{D^2 + 2\zeta\omega_n D + \omega_n^2}$$

and the equation defining the output for the range and azimuth accelerometers mounted in the nose is

$$\frac{a_{n,r}}{a_r + 4.5\dot{r}} = \frac{a_{n,a}}{a_a - 4.5\dot{q}} = \frac{\omega_n^2}{D^2 + 2\xi D\omega_n + \omega_n^2}$$

The accelerometers in the missile are sensitive only to the external forces, which in this case are the aerodynamic forces. Therefore, the acceleration terms to which the accelerometers respond in the range direction are

$$a_r = \frac{QA}{m}\left[C_{Z_\alpha}\left(\frac{v - V_Y}{V}\right) + C_{Z_\delta}\delta_r\right]$$

and in the azimuth direction are

$$a_a = \frac{QA}{m}\left[C_{Z_a}\left(\frac{w - V_Z}{V}\right) + C_{Z_\delta}\delta_a\right]$$

The constants associated with the control system are given in the following table:

Component	Value of gain or sensitivity constant	Value of damping ratio	Value of natural frequency, cps
Accelerometers (all)	1	0.6	30
Sensitivity K_1'	6		
Damping gain constant K_2' Acceleration feedback gain K_3'	6 -5		

APPENDIX B

SYSTEMS STABILITY COMPUTATIONS

For the analytical investigation of the integrating servosystem, the system was expressed as a transfer function of the ratio of the acceleration output to the command acceleration. The development of the transfer function a/a_i for the integrating servo is presented.

Consider the block diagram for the integrating servosystem (fig. 3) rearranged as shown in the following sketch:

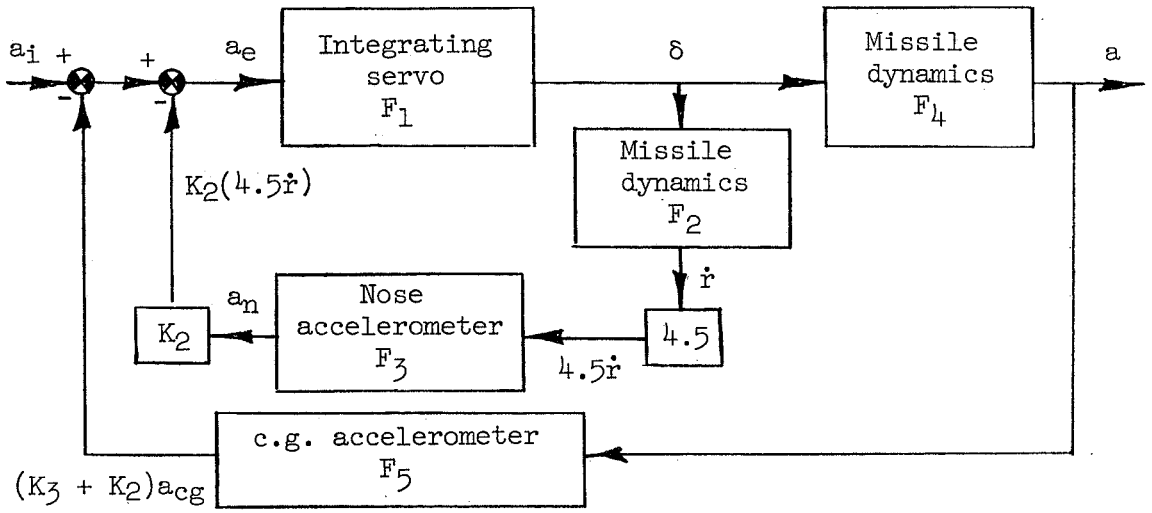

where F_1 to F_5 are the transfer functions for the various items and $K_3 + K_2 = 1$. This rearrangement is necessary so that the closed-loop transfer function of the inner loop can be evaluated and then used as a block in the outer loop, as shown in the following sketch:

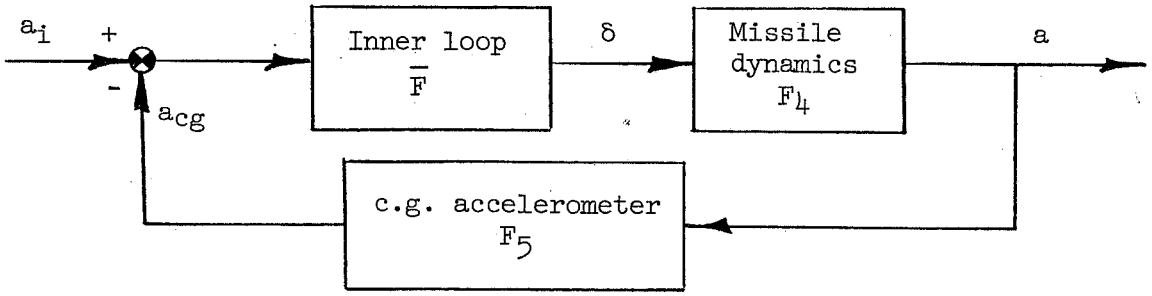

The expressions for the transfer functions are obtained by referring back to the expressions for these items given in appendix A. In this analysis the equations of motion of the missile were linearized and the velocity was considered constant. The expressions for the transfer functions are

$$F_1 = \frac{\delta}{a_e} = -\frac{K_1}{D}$$

L 1334

$$F_2 = \frac{\dot{r}}{\delta} = \frac{-\frac{QA}{m}\frac{d^2}{k^2}\frac{1}{d}C_{m_\delta}D^2 + \left(\frac{QA}{m}\right)^2\frac{d^2}{k^2}\frac{1}{dV}\left(C_{Z_\alpha}C_{m_\delta} - C_{Z_\delta}C_{m_\alpha}\right)D}{D^2 - \frac{QA}{mV}\left(C_{Z_\alpha} + \frac{1}{2}\frac{d^2}{k^2}C_{m_q}\right)D + \frac{QA}{m}\frac{d^2}{k^2}\left(\frac{QA}{m}\frac{1}{2V^2}C_{Z_\alpha}C_{m_q} - \frac{1}{d}C_{m_\alpha}\right)}$$

$$F_3 = \frac{a_n}{4.5\dot{r}} = \frac{\omega_n^2}{D^2 + 2\zeta\omega_n D + \omega_n^2}$$

$$F_4 = \frac{a}{\delta} = \frac{\frac{QA}{m}\left[C_{Z_\delta}D^2 - \frac{1}{2}\frac{QA}{m}\frac{d^2}{k^2}C_{Z_\delta}C_{m_q}D + \frac{QA}{m}\frac{d^2}{k^2}\left(C_{Z_\alpha}C_{m_\delta} - C_{Z_\delta}C_{m_\alpha}\right)\right]}{D^2 - \frac{QA}{mV}\left(C_{Z_\alpha} + \frac{1}{2}\frac{d^2}{k^2}C_{m_q}\right)D + \frac{QA}{m}\frac{d^2}{k^2}\left(\frac{QA}{m}\frac{1}{2V^2}C_{Z_\alpha}C_{m_q} - \frac{1}{d}C_{m_\alpha}\right)}$$

$$F_5 = \frac{a_{cg}}{a} = \frac{\omega_n^2}{D^2 + 2\zeta\omega_n D + \omega_n^2}$$

The transfer functions F_3 and F_5 are the same because accelerometers with the same characteristics were used at the two locations. The expression for the closed-loop transfer function of the inner loop $\overline{F}$ is

$$\overline{F} = \frac{F_1}{1 + 4.5K_2F_1F_2F_3}$$

Substitution of the functions for F_1, F_2, and F_3 and simplifying results in the following expression for $\overline{F}$:

$$\overline{F} = \frac{\left\{ -K_1 \left\{ D^4 + \left[2\zeta\omega_n - \frac{QA}{mV}\left(C_{Z_\alpha} + \frac{1}{2}\frac{d^2}{k^2} C_{m_q} \right) \right] D^3 \right.\right.}{\left.\left. + \left[\omega_n^2 - 2\zeta\omega_n \frac{QA}{mV}\left(C_{Z_\alpha} + \frac{1}{2}\frac{d^2}{k^2} C_{m_q} \right) + \frac{QA}{m}\frac{d^2}{k^2}\left(\frac{QA}{m}\frac{1}{2V^2} C_{Z_\alpha} C_{m_q} - \frac{1}{d} C_{m_\alpha} \right) \right] D^2 \right.\right.}$$
$$\left.\left. + \left[-\omega_n^2 \frac{QA}{mV}\left(C_{Z_\alpha} + \frac{1}{2}\frac{d^2}{k^2} C_{m_q} \right) + 2\zeta\omega_n \frac{QA}{m}\frac{d^2}{k^2}\left(\frac{QA}{m}\frac{1}{2V^2} C_{Z_\alpha} C_{m_q} - \frac{1}{d} C_{m_\alpha} \right) \right] D \right.$$
$$\left. + \omega_n^2 \frac{QA}{m}\frac{d^2}{k^2}\left(\frac{QA}{m}\frac{1}{2V^2} C_{Z_\alpha} C_{m_q} - \frac{1}{d} C_{m_\alpha} \right) \right\}$$
$$\overline{\left\{ D\left[D^2 - \frac{QA}{mV}\left(C_{Z_\alpha} + \frac{1}{2}\frac{d^2}{k^2} \right) D + \frac{QA}{m}\frac{d^2}{k^2}\left(\frac{QA}{m}\frac{1}{2V^2} C_{Z_\alpha} C_{m_q} - \frac{1}{d} C_{m_\alpha} \right) \right] \right.}$$
$$\left. - 4.5 K_1 K_2 \omega_n^2 \left[-\frac{QA}{m}\frac{d^2}{k^2}\frac{1}{d} C_{m_\delta} D^2 + \left(\frac{QA}{m} \right)^2 \frac{d^2}{k^2}\frac{1}{dV}\left(C_{Z_\alpha} C_{m_\delta} - C_{Z_\delta} C_{m_\alpha} \right) D \right] \right\}$$

L 1334

The expression for the closed-loop transfer function of the outer loop a/a_i is

$$\frac{a}{a_i} = \frac{F_4 \overline{F}}{1 + F_4 F_5 \overline{F}}$$

Substitution of the functions for F_4, F_5, and $\overline{F}$ into a/a_i and simplifying results in the following expression:

$$\frac{a}{a_i} = \frac{-K_1\left(E_1 D^4 + E_2 D^3 + E_3 D^2 + E_4 D + E_5 \right)}{D^5 + B_1 D^4 + B_2 D^3 + B_3 D^2 + B_4 D + B_5}$$

where

$$E_1 = \frac{QA}{m} C_{Z_\delta}$$

$$E_2 = \frac{QA}{m} 2\zeta\omega_n C_{Z_\delta} - \left(\frac{QA}{m}\right)^2 \frac{d^2}{k^2} \frac{1}{2V} C_{Z_\delta} C_{m_q}$$

$$E_3 = \frac{QA}{m} \omega_n{}^2 C_{Z_\delta} - \left(\frac{QA}{m}\right)^2 \frac{d^2}{k^2} \frac{1}{2V} 2\zeta\omega_n C_{Z_\delta} C_{m_q} + \left(\frac{QA}{m}\right)^2 \frac{d^2}{k^2} \frac{1}{d}\left(C_{Z_\alpha} C_{m_\delta} - C_{Z_\delta} C_{m_\alpha}\right)$$

$$E_4 = -\left(\frac{QA}{m}\right)^2 \frac{d^2}{k^2} \frac{1}{2V} \omega_n{}^2 C_{Z_\delta} C_{m_q} + \left(\frac{QA}{m}\right)^2 \frac{d^2}{k^2} \frac{1}{d} 2\zeta\omega_n \left(C_{Z_\alpha} C_{m_\delta} - C_{Z_\delta} C_{m_\alpha}\right)$$

$$E_5 = \left(\frac{QA}{m}\right)^2 \frac{d^2}{k^2} \frac{1}{d} \omega_n{}^2 \left(C_{Z_\alpha} C_{m_\delta} - C_{Z_\delta} C_{m_\alpha}\right)$$

and

$$B_1 = 2\zeta\omega_n - \frac{QA}{m} \frac{1}{V}\left(C_{Z_\alpha} + \frac{1}{2} \frac{d^2}{k^2} C_{m_q}\right)$$

$$B_2 = \omega_n{}^2 - \frac{QA}{m} \frac{1}{V} 2\zeta\omega_n \left(C_{Z_\alpha} + \frac{1}{2} \frac{d^2}{k^2} C_{m_q}\right) - \frac{QA}{m} \frac{d^2}{k^2} \frac{1}{2} C_{m_\alpha} + \left(\frac{QA}{m}\right)^2 \frac{d^2}{k^2} \frac{1}{V^2} C_{Z_\alpha} C_{m_q}$$

$$B_3 = \frac{QA}{m}\left[-2\zeta\omega_n \frac{d^2}{k^2} \frac{1}{d} C_{m_\alpha} + K_1 \omega_n{}^2 \left(4.5 K_2 \frac{d^2}{k^2} \frac{1}{d} C_{m_\delta} - C_{Z_\delta}\right)\right]$$
$$- \frac{QA}{m} \frac{\omega_n{}^2}{V}\left(C_{Z_\alpha} + \frac{1}{2} \frac{d^2}{k^2} C_{m_q}\right) + \left(\frac{QA}{m}\right)^2 \frac{d^2}{k^2} \frac{1}{2V^2} 2\zeta\omega_n C_{Z_\alpha} C_{m_q}$$

$$B_4 = - \frac{QA}{m} \frac{d^2}{k^2} \frac{\omega_n^2}{d} C_{m_\alpha} + \left(\frac{QA}{m}\right)^2 \frac{d^2}{k^2} \frac{1}{2V^2} \frac{\omega_n^2}{d} C_{Z_\alpha} C_{m_q}$$

$$+ \left(\frac{QA}{m}\right)^2 \frac{d^2}{k^2} \frac{\omega_n^2}{Vd} K_1 \left[\frac{d}{2} C_{Z_\delta} C_{m_q} - 4.5 K_3 \left(C_{Z_\alpha} C_{m_\delta} - C_{Z_\delta} C_{m_\alpha} \right) \right]$$

$$B_5 = - \left(\frac{QA}{m}\right)^2 \frac{d^2}{k^2} \frac{\omega_n^2}{d} K_1 \left(C_{Z_\alpha} C_{m_\delta} - C_{Z_\delta} C_{m_\alpha} \right)$$

L
1
3
3
4

REFERENCES

1. Tobak, Murray, and Wehrend, William R.: Stability Derivatives of Cones at Supersonic Speeds. NACA TN 3788, 1956.

2. Seaberg, Ernest C., Sproull, Royce H., and Reid, H. J. E., Jr.: Flight Investigation at Supersonic Mach Numbers of an Automatic Acceleration Control Missile in Which Rate Damping is Obtained From a Linear Accelerometer Placed Ahead of the Missile Center of Gravity. NACA RM L55G29, 1955.

3. Gloria, Hermilo R.: An Experimental Investigation of the Static Longitudinal Stability and Control Characteristics of a Wingless Missile Configuration at Mach Numbers From 3.0 to 6.3. NACA RM A58C20, 1958.

TABLE I.- MASS AND AERODYNAMIC CONSTANTS FOR THE MISSILE AND INITIAL CONDITIONS FOR THE COMPUTATIONS

Mass and aerodynamic constants:	
m, slugs	108
I_X, slug-ft^2	80
I_Y, slug-ft^2	900
A, sq ft	6.1
d, ft	2.79
$C_{X,\alpha=0^\circ}$	-0.576
C_{Z_α}, per radian	-3.967
C_{Z_δ}, per radian	0.661
C_{m_α}, per radian	-1.13
C_{m_δ}, per radian	1.085
C_{m_q}	-14.99
Initial conditions:	
y, ft	400,000
θ, deg	-22.5
V, ft/sec	21,018.5
$\dot{x}$, ft/sec	19,420
$\dot{y}$, ft/sec	-8,040

TABLE II.- CONDITIONS FOR THE IMPACT-POINT COMPUTATIONS

Run number	Reentry condition	Range command	Azimuth command	Data in figure -
1	No earth rotation	None	None	10, 11
2	Against earth rotation			
3	With earth rotation			
4	Perpendicular to earth rotation			
5	No earth rotation	0	0	12(a)
6	Against earth rotation			12(b)
7	With earth rotation			12(c)
8	Perpendicular to earth rotation			12(d)
9	No earth rotation	2		12(a)
10		5		
11		10		
12		-5		
13		-10		
14		10	5	
15		5		
16		0		
17		-5		
18		10	10	
19		0		
20		-10		
21	Against earth rotation	2	0	12(b)
22		5		
23		10		
24		-5		
25		-10		
26		10	5	
27		5		
28		0		
29		-5		
30		10	10	
31		0		
32		-10		
33	With earth rotation	2	0	12(c)
34		5		
35		10		
36		-5		
37		-10		
38		10	5	
39		5		
40		0		
41		-5		
42		10	10	
43		0		
44		-10		
45	Perpendicular to earth rotation	2	0	12(d)
46		5		
47		10		
48		-5		
49		-10		
50		10	5	
51		5		
52		0		
53		-5		
54		10	10	
55		5		
56		0		
57		-10		
58		10	-5	
59		5		
60		0		
61		-5		
62		10	-10	
63		0		
64		-10		

TABLE III.- CONDITIONS FOR WHICH THE STABILITY COMPARISON WAS MADE

Condition	Altitude, ft	Q, lb/sq ft	V, ft/sec	Mach number
1	40,763	49,081	13,182	13.60
2	10,272	12,098	3,730	11.21
3	90,327	10,238	20,256	20.54
4	101,346	6,260	20,602	20.44
5	19	4,234	1,910	1.71
6	200,000	124	21,018	20.00

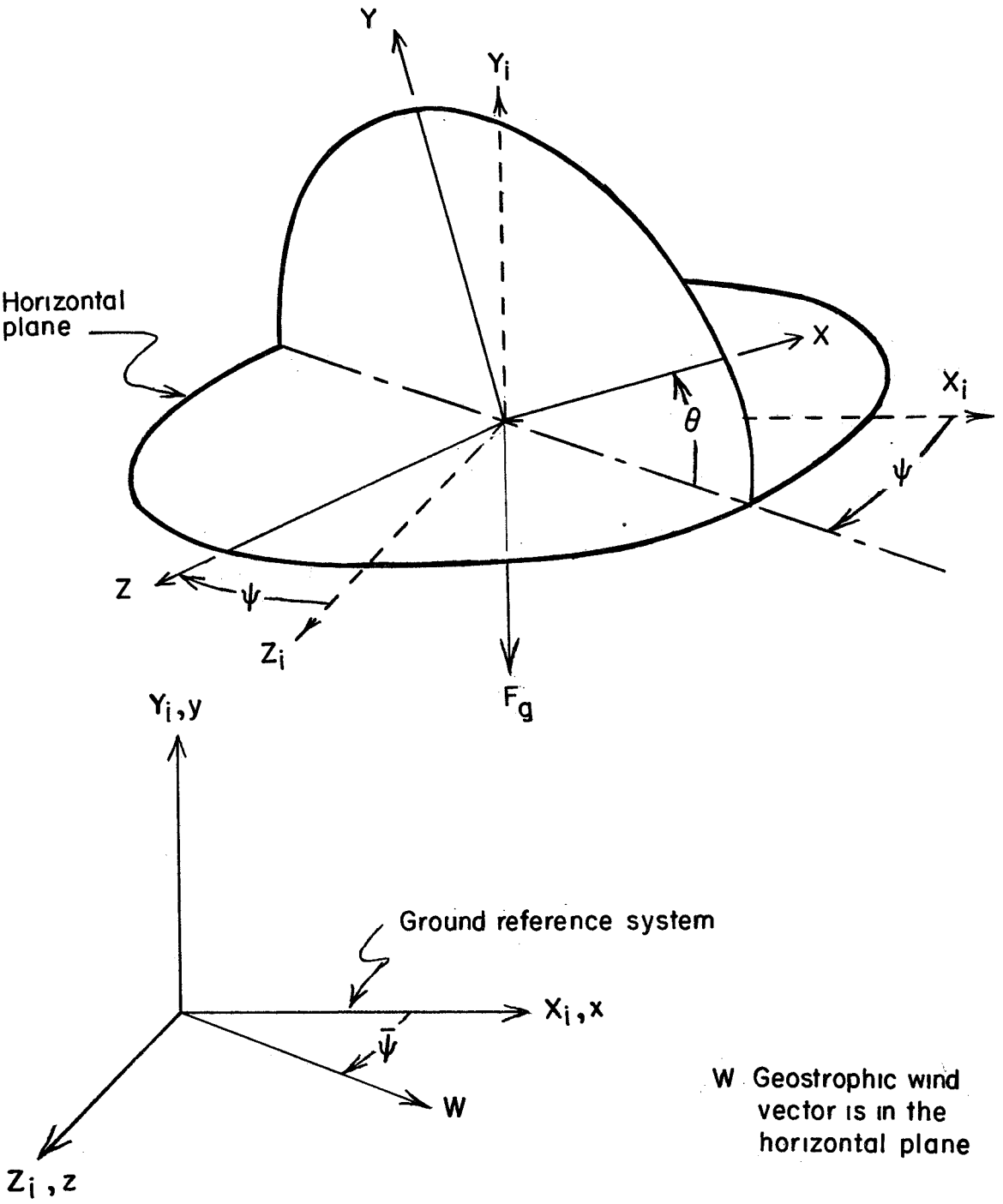

Figure 1.- Axis system used in this analysis.

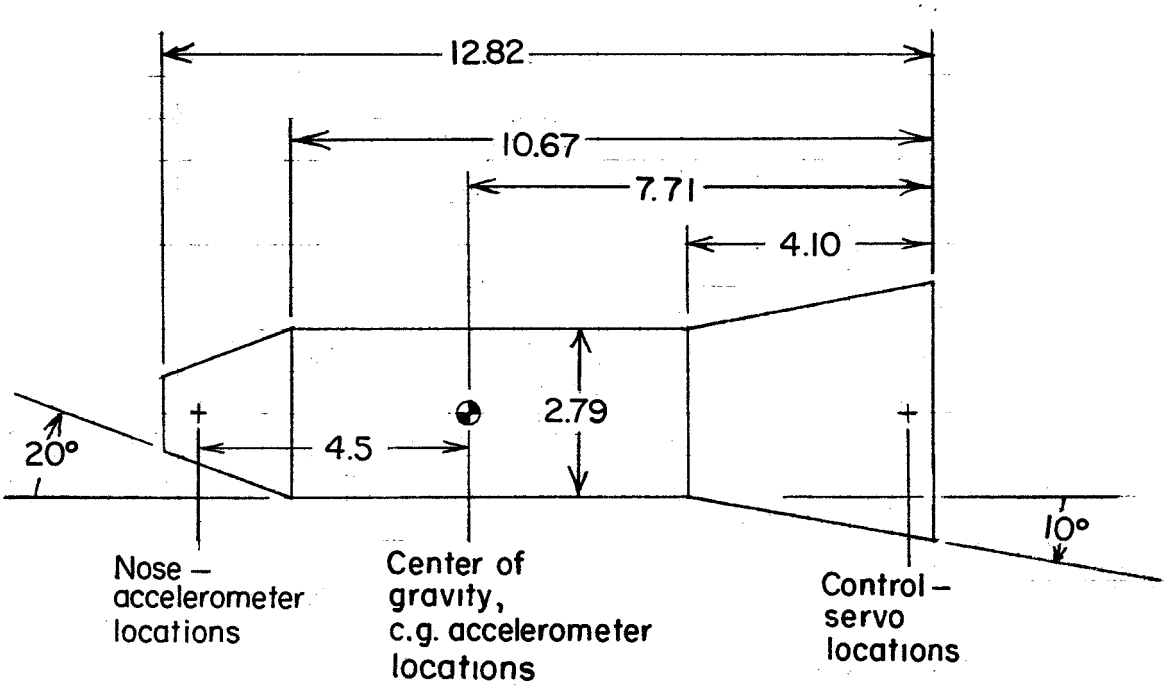

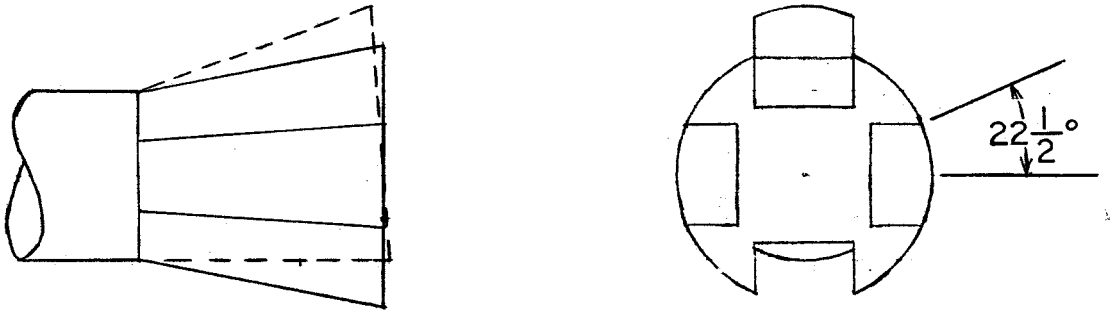

Detail of control deflection

Figure 2.- Sketch showing missile and location of control components. Dimensions are in feet unless otherwise specified.

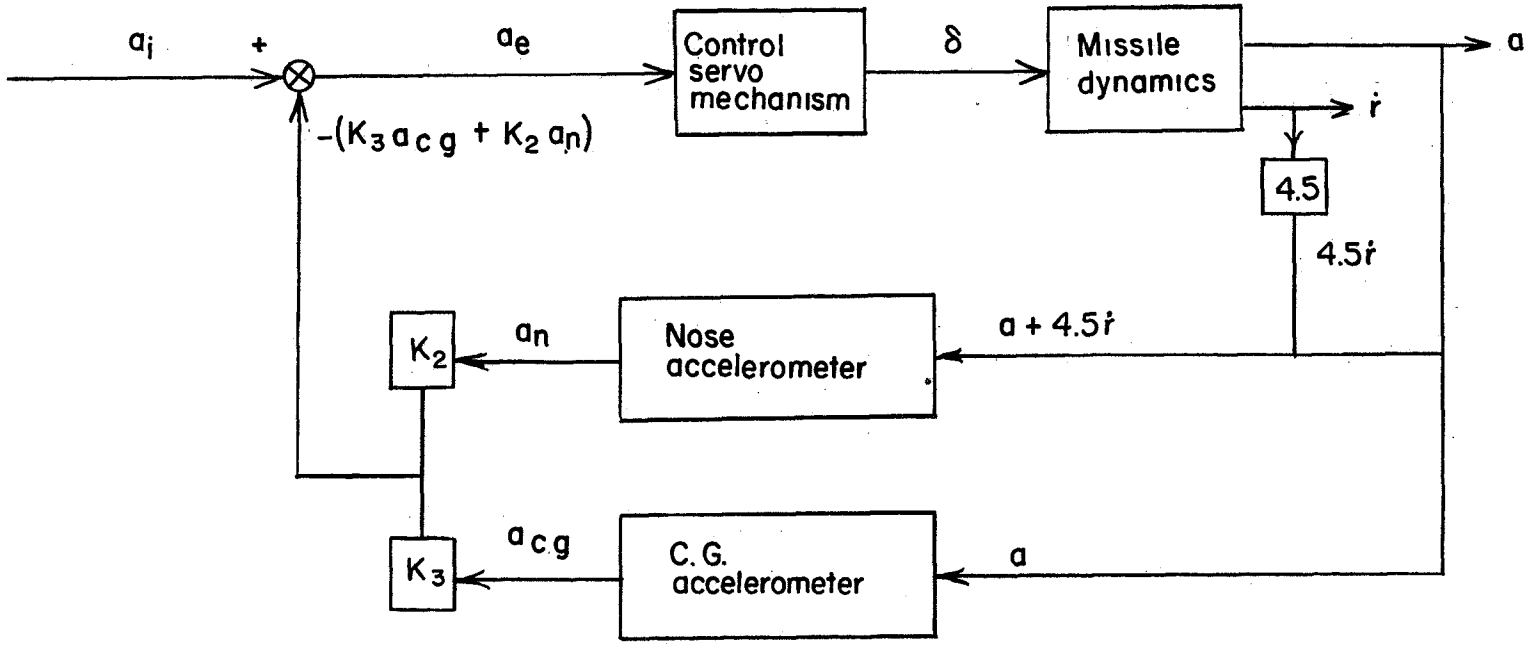

Figure 3.- Block diagram of the range-control system. The azimuth-control system is identical to this range system. Transfer functions for the various blocks are given in appendix B.

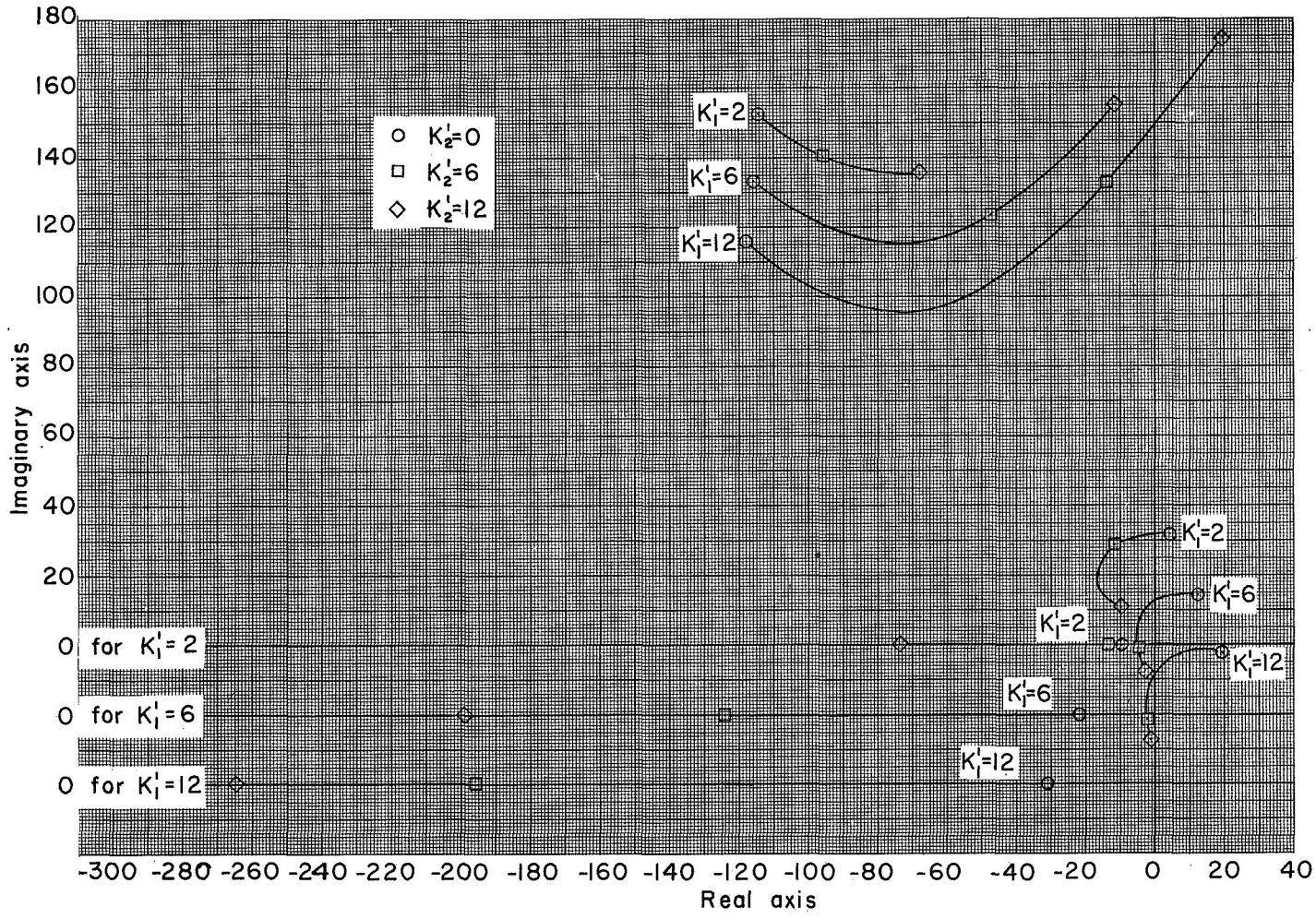

Figure 4.- Loci of roots in the complex plane for three forward loop sensitivities $\left(K_1' = 2, 6, 12\right)$ and a range of damping gain constants $\left(0 - K_2' - 12\right)$. Q = 49,081 lb/sq ft; altitude of 40,763 feet. Note that zeros are shifted for each locus.

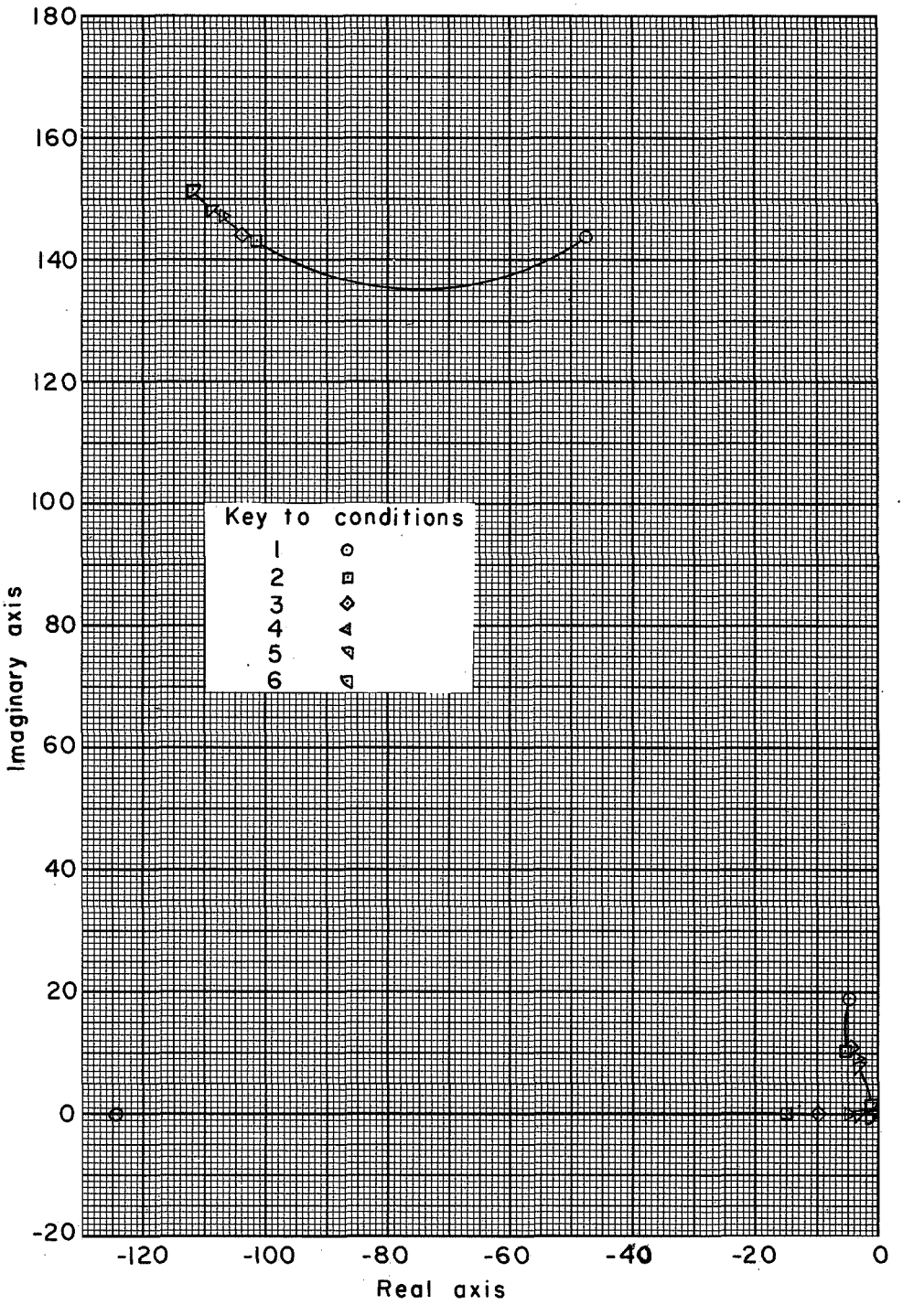

Figure 5.- Loci of roots for $K_1' = 6$ and $K_2' = 6$ for the six flight conditions listed in table III.

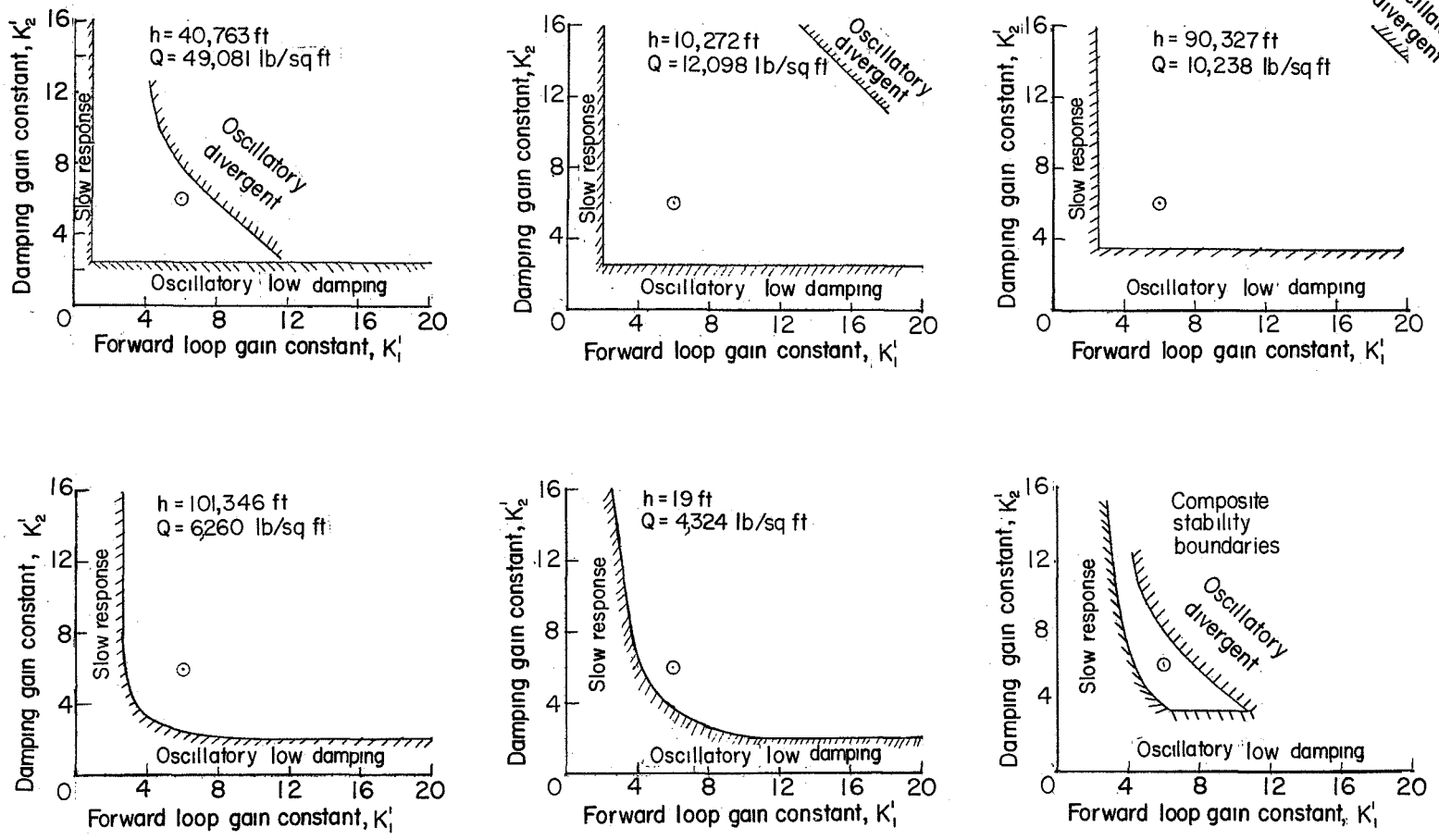

Figure 6.- Stability boundaries for the integrating servosystem for five representative flight conditions as obtained from an analog computer study. Symbol represents gain constants used in the investigation.

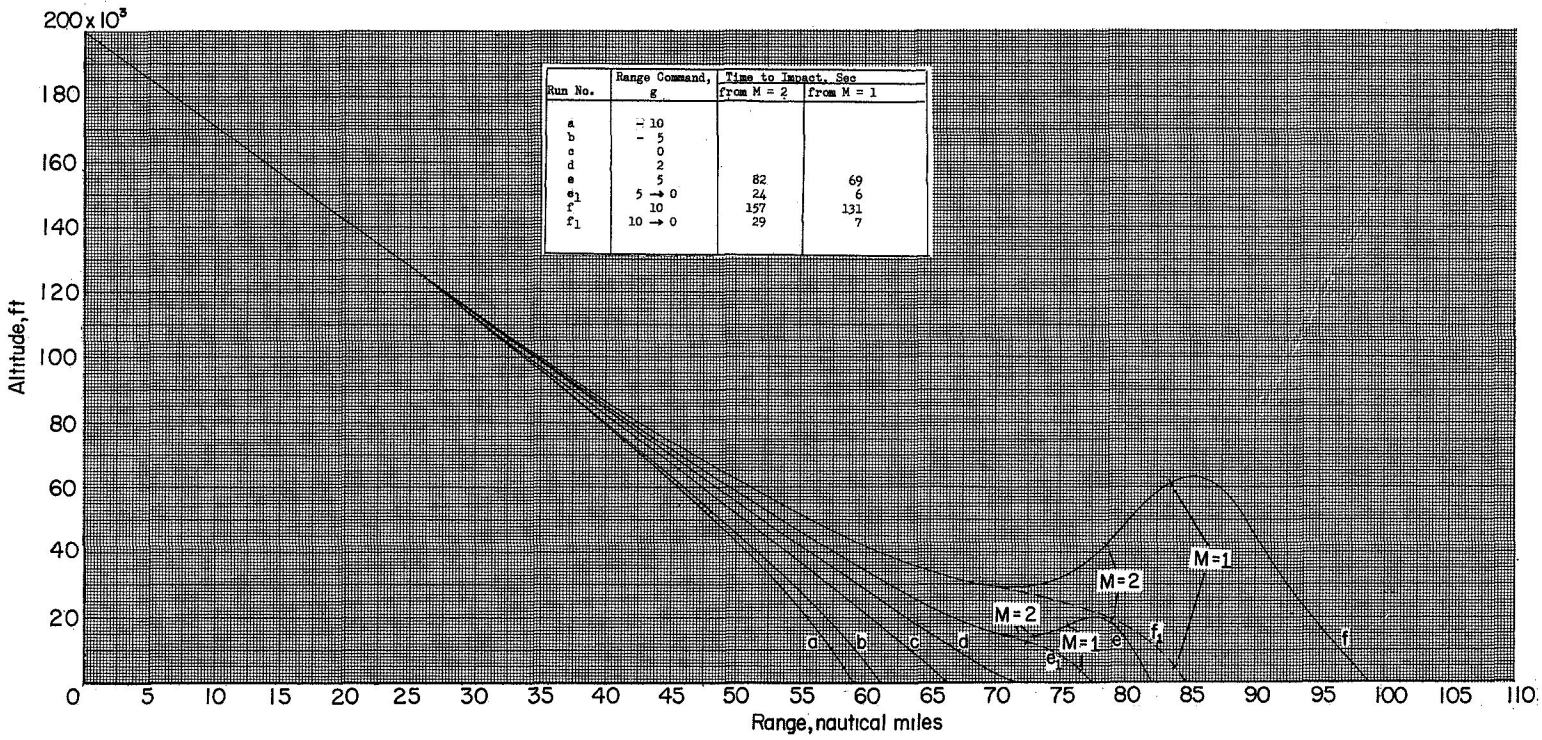

Run No.	Range Command, g	Time to Impact, Sec from M = 2	Time to Impact, Sec from M = 1
a	∞ 10		
b	- 5		
c	0		
d	2		
e	5	82	69
e_1	5 → 0	24	6
f	10	157	131
f_1	10 → 0	29	7

Figure 7.- Trajectory profiles for various amounts of range command for a condition with no earth-rotation effects. Range was computed for an earth-fixed-axis system.

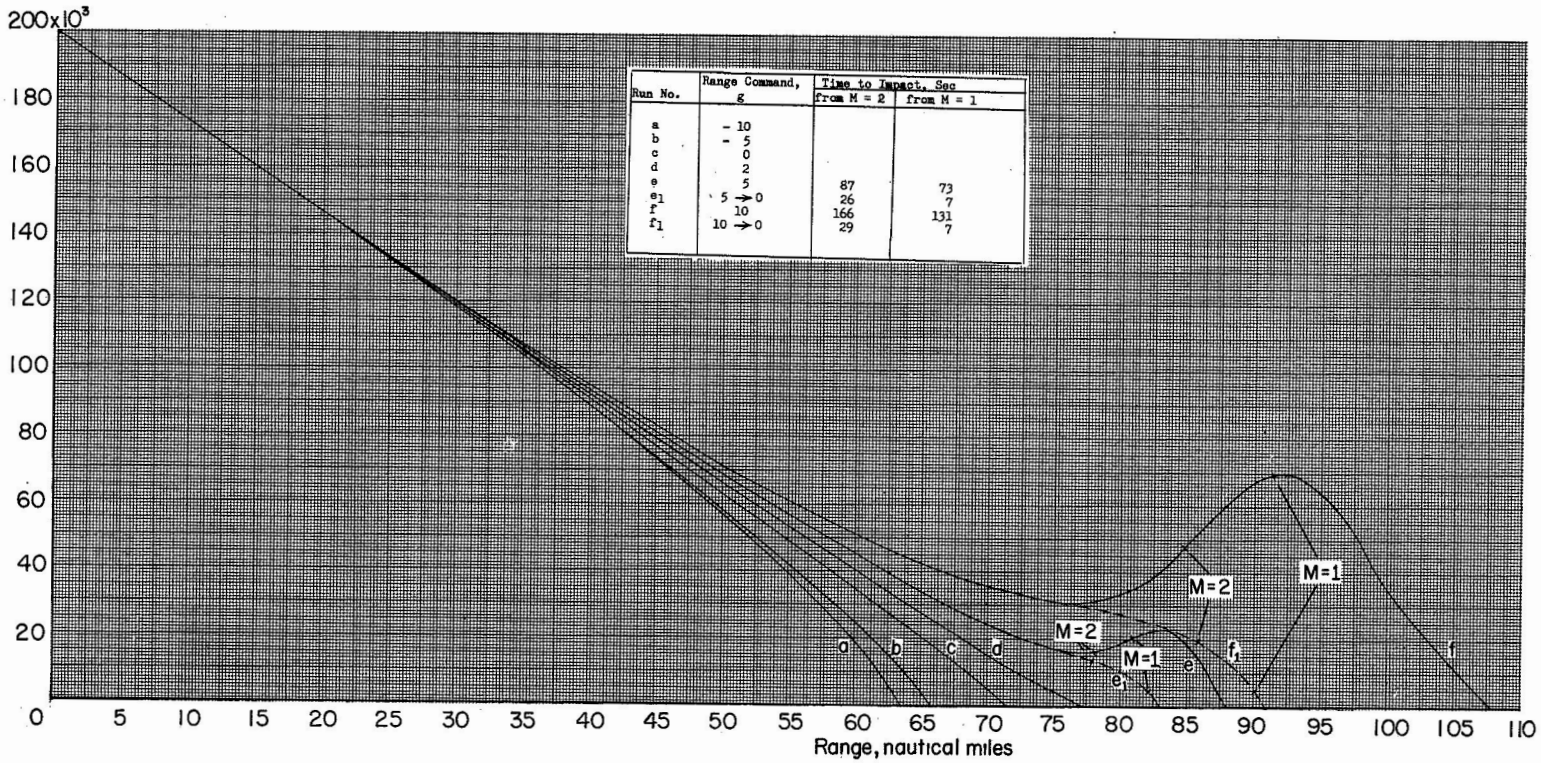

Figure 8.- Trajectory profiles for various amounts of range command for reentry at the equator against the earth rotation. Range was computed for an earth-fixed-axis system.

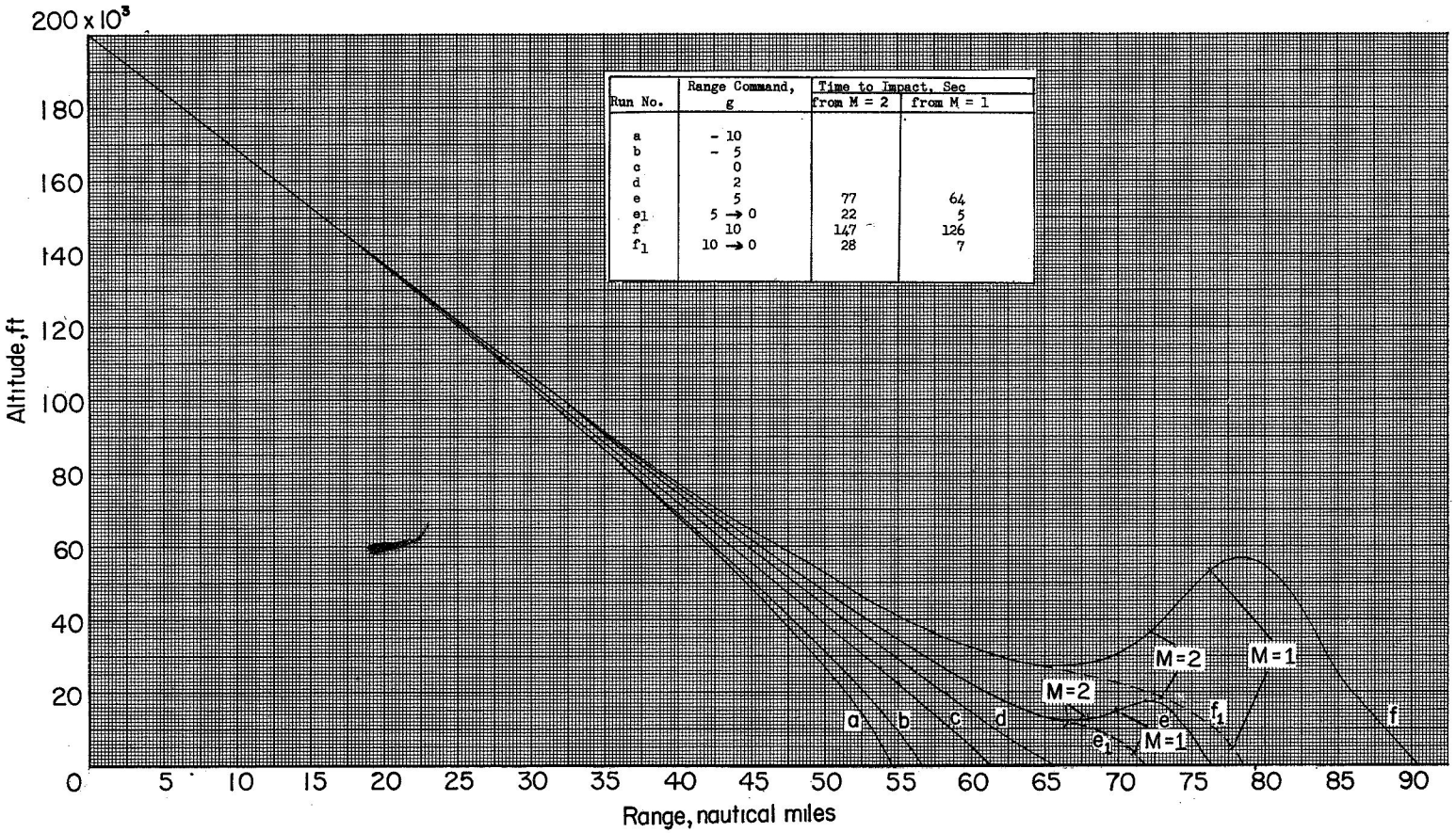

Run No.	Range Command, g	Time to Impact, Sec from M = 2	Time to Impact, Sec from M = 1
a	- 10		
b	- 5		
c	0		
d	2		
e	5	77	64
e1	5 → 0	22	5
f	10	147	126
f1	10 → 0	28	7

Figure 9.- Trajectory profiles for various amounts of range command for reentry at the equator in the same direction as the earth rotation. Range was computed for an earth-fixed-axis system.

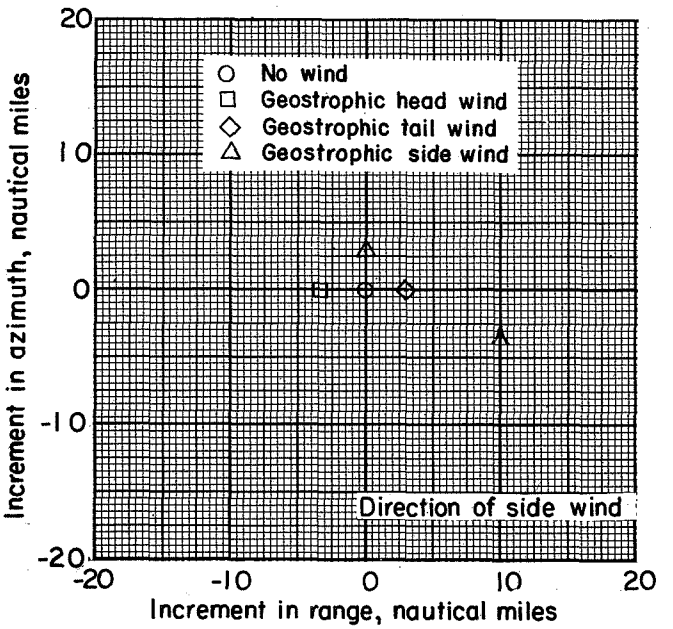

Figure 10.- Drift of impact point due to geostrophic wind. Inertial axis system.

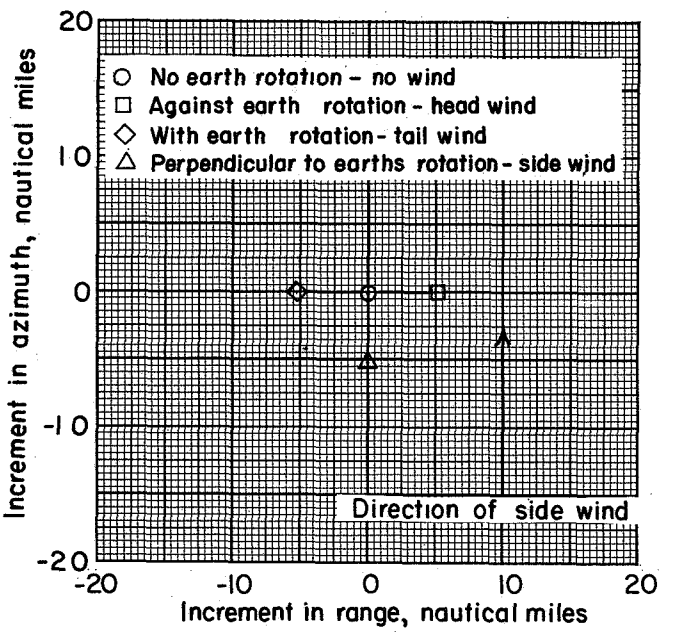

Figure 11.- Displacement of impact point due to geostrophic wind and earth rotation. Earth-fixed-axis system.

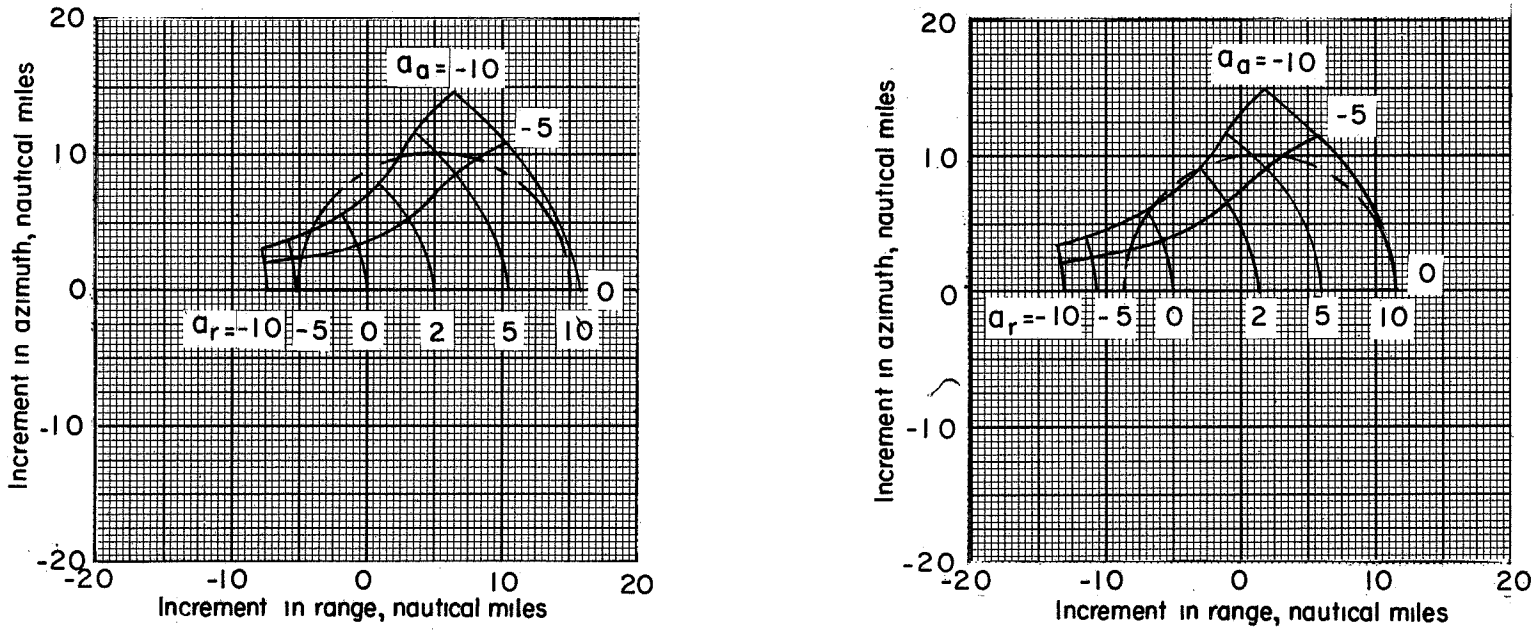

(a) No earth rotation or wind.

(b) Against earth rotation, head wind.

Figure 12.- Map of the displacement of the impact point with control command for an earth-fixed-axis system for various reentry conditions. a_r and a_a are indicated in g units. Dashed circle represents a radius of 10 nautical miles from the impact point of $a_r = 2$, $a_a = 0$.

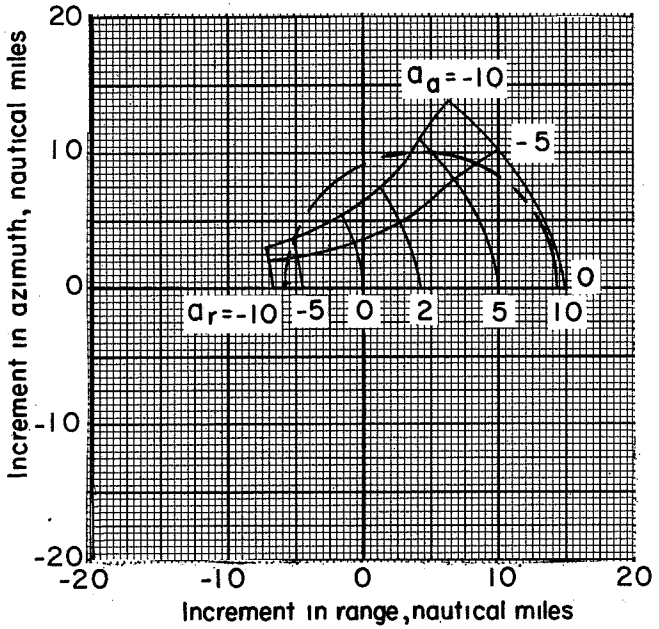

(c) Same direction as earth rotation, tail wind.

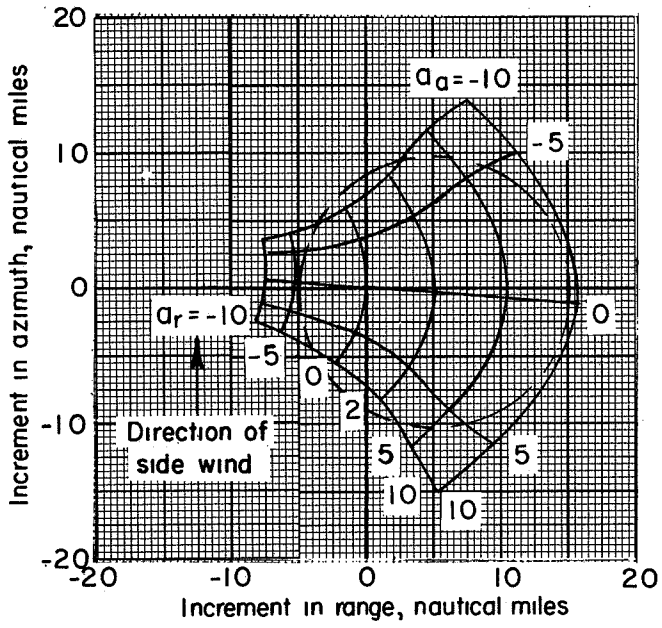

(d) Perpendicular to earth rotation, side wind.

Figure 12.- Concluded.